Shaping frequency-entangled qudits

Christof Bernhard,* Bänz Bessire,* Thomas Feurer, and André Stefanov†
Institute of Applied Physics, University of Bern, 3012 Bern, Switzerland
(Received 28 May 2013; published 23 September 2013)

We demonstrate the creation, characterization, and manipulation of frequency-entangled qudits by shaping the energy spectrum of entangled photons. The generation of maximally entangled qudit states is verified up to dimension $d = 4$ through tomographic quantum-state reconstruction. Subsequently, we measure Bell parameters for qubits and qutrits as a function of their degree of entanglement. In agreement with theoretical predictions, we observe that for qutrits the Bell parameter is less sensitive to a varying degree of entanglement than for qubits. For frequency-entangled photons, the dimensionality of a qudit is ultimately limited by the bandwidth of the pump laser and can be on the order of a few millions.

DOI: 10.1103/PhysRevA.88.032322 PACS number(s): 03.67.Bg, 03.65.Ud, 03.65.Wj, 42.50.Dv

I. INTRODUCTION

Entanglement [1] is one of the most intriguing features of quantum theory and is a fundamental resource for quantum information processing. It was experimentally revealed by the observation of correlations with no classical origins. Through Bell inequalities, the nonlocality of nature was tested by numerous experiments using entangled two-dimensional states (qubits) [2]. Both fundamental tests of quantum theory and applications benefit greatly from entanglement in higher dimensions. Entangling d-dimensional states denoted as qudits allows to formulate generalized Bell inequalities, which are more resistant to noise than their two-dimensional predecessors [3,4]. In loophole-free Bell experiments the detection efficiency threshold can be lowered [5]. Finally, both the effective bit rate of quantum key distribution and the robustness to errors can be increased [6]. These examples, among others, stimulated research towards different schemes to generate and manipulate photonic qudits in high dimensions.

Due to their low decoherence rate, photons are used in many experiments as a robust carrier of entanglement. Photonic entangled states are usually produced by the nonlinear interaction of spontaneous parametric down conversion (SPDC). The coherence of this process, together with conservation rules, can generate entanglement in the finite Hilbert space of polarization modes [7]. Entanglement in infinite spaces can be realized for transverse (momentum) or orbital angular momentum (OAM) modes [8–14] and for energy-time states [15]. The amount of entanglement is commonly quantified by the Schmidt number K. For transverse-wave-vector entanglement, K is on the order of 10 for perfect SPDC phase-matching conditions [16], approximately 400 for specific nonperfect phase-matching conditions [9], and approximately 50 for OAM entanglement [14]. Similar Schmidt numbers can be achieved in energy-time entanglement generated by short pump pulses [15,17], but much larger K numbers are obtained for a quasimonochromatic pump laser. In practice, the infinite Hilbert space is projected onto a finite space of, for example, discrete time or frequency bins. In the time-bin subspace two-photon interferences for $d = 3,4$ have been observed by interferometers with multiple arms [18,19]. This, however, requires interferometric stability and becomes very complex for higher dimensions. In the frequency-bin subspace, interferences between two entangled photons, each in an effective two-dimensional space, have been observed by manipulating the spectra with a combination of narrow-band filters and electro-optic modulators [20]. Some of the aforementioned experiments are very useful for quantum key distribution because frequency is the most suitable degree of freedom of light to distribute entanglement over a large distance through optical fibers [21]. However, these experiments do not provide sufficient control of the phase and amplitude of qudits in the frequency domain to extensively study the properties of d-dimensional states with $d > 2$.

In this article, we demonstrate a methodology that allows for full control over entangled qudits through coherent modulation of the photon spectra. It is derived from a classical pulse-shaping arrangement and contains a spatial light modulator (SLM) as a reconfigurable modulation tool. This technique is widely used in ultrafast optics [22] and has been adapted to manipulate the wave function of energy-time entangled two-photon states [23,24]. The flexibility of the experimental setup allowed to reconstruct the density matrices of maximally entangled qudits up to $d = 4$. Moreover, we demonstrate the presence of energy-time entanglement by measuring a Bell parameter above the local variable limit for maximally and certain nonmaximally entangled qubit and qutrit states.

II. EXPERIMENTAL SETUP

Figure 1 depicts a schematic of the experimental setup. The entangled photons are generated in a type-0 SPDC process where all involved photons, the pump, the created idler (i), and signal (s), are identically polarized [25]. For this purpose we pump a 11.5-mm-long positive uniaxial and periodically poled nonlinear $KTiOPO_4$ (PPKTP) crystal with a poling periodicity of 9 μm by means of a quasimonochromatic Nd:YVO_4 (Coherent Verdi V5) laser centered at 532 nm featuring a narrow spectral bandwidth of about 5 MHz. The collinear pump beam is focused into the middle of the PPKTP crystal with a power of 5 W. To compensate for group-velocity dispersion in the setup and to allow for coherent shaping of the spectra, the idler and signal photon are imaged through a prism

*These authors contributed equally to this work.
†Author to whom correspondence should be addressed: andre.stefanov@iap.unibe.ch

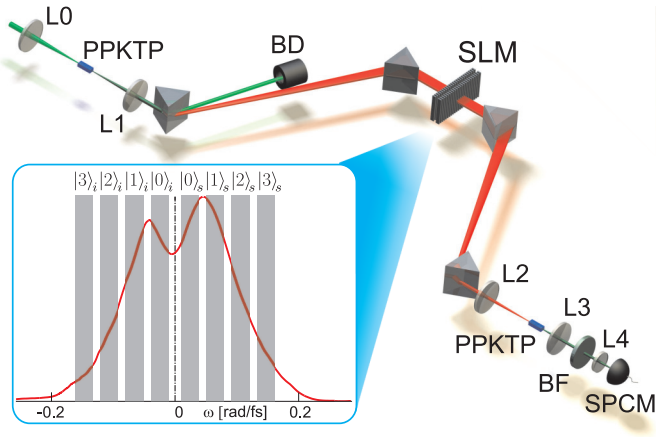

FIG. 1. (Color online) Schematic of the experimental setup and frequency-bin structure. L0, pump beam focusing lens ($f = 150$ mm); PPKTP, nonlinear crystal; BD, beam dump; SLM, spatial light modulator; L1 and L2, two-lens symmetric imaging arrangement ($f = 100$ mm) to enhance the spectral resolution with a magnification of 1:6 at the symmetry axis of the four-prisms compressor; BF, bandpass filter; SPCM, single-photon counting module with a two-lens (L3, L4) imaging system. The inset shows the measured down-converted spectrum overlaid with a schematic illustration of the frequency bins for a ququart. Each of the gray shaded areas represents a single bin whose amplitude and phase can be manipulated individually.

compressor arrangement composed of four N-SF 11 equilateral prisms, where the first prism deflects the residue of the pump into a beam dump. At the symmetry axis between the second and the third prism a SLM (Jenoptik, SLM-S640d) is aligned along the spatially dispersed down-converted spectrum. This device consists of two similar nematic liquid-crystal arrays of 640 pixels, each with a width of 100 μm and separated by a gap of 3 μm. The orientation of the liquid-crystal molecules within a pixel can be controlled by the applied voltage. Together with a linearly polarized input beam and a polarization-dependent detection scheme, the phase and amplitude of the transmitted frequencies at each pixel can be modulated. Coincidences of the entangled photon pairs are detected within a time window of about 100 fs through up conversion in a second PPKTP crystal [23]. The up-converted 532 nm photons are then imaged onto the active area of a single-photon counting module (SPCM, ID Quantique, id100-50-uln) whereas the residual photons around 1064 nm are suppressed by a bandpass filter (4 mm BG18). In principle, sum frequency generation between one photon and a femtosecond laser pulse would realize a fast optical gating, allowing to perform a fast coincidence detection on spatially separated photons.

III. THEORY

Restricting the configuration of the three photons to the case where they are mutually collinear, the entangled two-photon state can be written as

$$|\psi\rangle = \int_{-\infty}^{\infty}\int_{-\infty}^{\infty} d\omega_i d\omega_s \Gamma(\omega_i,\omega_s)\hat{a}_i^\dagger(\omega_i)\hat{a}_s^\dagger(\omega_s)|0\rangle_i|0\rangle_s, \quad (1)$$

where $\Gamma(\omega_i,\omega_s) = \alpha(\omega_i,\omega_s)\Phi(\omega_i,\omega_s)$. It depends on the pump envelope function $\alpha(\omega_i,\omega_s)$ and on $\Phi(\omega_i,\omega_s)$ which describes the joint spectral amplitude of SPDC filtered by the phase-matching properties of the detection crystal. Idler and signal photons with corresponding relative frequency $\omega_{i,s}$ are created by the operators $\hat{a}_{i,s}^\dagger(\omega_{i,s})$, acting on the combined vacuum state $|0\rangle_i|0\rangle_s$. We have calculated the entropy of entanglement [26] E of $\Gamma(\omega_i,\omega_s)$ to be $E = (21.1 \pm 0.2)$ ebits for a pump bandwidth of 5 MHz and experimental parameters of the SPDC and the detection crystal by means of a numerical approximation method [27]. This amount of entropy is the same as in a maximally entangled qudit state with $d = 2^E \approx 2.2 \times 10^6$. As a further quantification of entanglement, the Schmidt number K has been computed numerically to be $K \approx 1.3 \times 10^6$. In order to use this large resource of entanglement for quantum information processing, we encode qudits in the frequency domain by projecting the state $|\psi\rangle$ into a discrete d^2-dimensional subspace spanned by the states $|j\rangle_i|k\rangle_s$ with $|j\rangle_{i,s} \equiv \int_{-\infty}^{\infty} d\omega f_j^{i,s}(\omega)\hat{a}_{i,s}^\dagger(\omega)|0\rangle_{i,s}$ and $j = 0,\ldots,d-1$. The projected state is then expressed by

$$|\psi\rangle^{(d)} = \sum_{j=0}^{d-1}\sum_{k=0}^{d-1} c_{jk}|j\rangle_i|k\rangle_s, \quad (2)$$

with $c_{jk} = \int_{-\infty}^{\infty}\int_{-\infty}^{\infty} d\omega_i d\omega_s f_j^{i*}(\omega_i) f_k^{s*}(\omega_s)\Gamma(\omega_i,\omega_s)$ and the orthogonality condition $\int_{-\infty}^{\infty} d\omega f_j^{i,s*}(\omega) f_k^{i,s}(\omega) = \delta_{jk}$. For the experiments presented here, we specifically define frequency bins according to

$$f_j^{i,s}(\omega) = \begin{cases} 1/\sqrt{\Delta\omega_j} & \text{for} \quad |\omega - \omega_j| < \Delta\omega_j, \\ 0 & \text{otherwise.} \end{cases} \quad (3)$$

Imposing $|\omega_j - \omega_k| > (\Delta\omega_j + \Delta\omega_k)/2$ for all j,k ensures that adjacent bins do not overlap. For simplicity, we assume in the following a continuous-wave pump by $\alpha(\omega_i,\omega_s) \propto \delta(\omega_i + \omega_s)$ and therefore $|\psi\rangle^{(d)}$ becomes restricted to its diagonal form,

$$|\psi\rangle^{(d)} = \sum_{j=0}^{d-1} c_j|j\rangle_i|j\rangle_s. \quad (4)$$

Experimentally, the amplitude and phase of each spectral component of the idler and signal photon can be adjusted with the SLM (Fig. 1). The effect on each photon is described by a complex transfer function $M^{i,s}(\omega)$. A frequency-bin structure according to Eq. (3) is then implemented through

$$M^{i,s}(\omega) = \sum_{j=0}^{d-1} u_j^{i,s} f_j^{i,s}(\omega) = \sum_{j=0}^{d-1} |u_j^{i,s}| e^{i\phi_j^{i,s}} f_j^{i,s}(\omega), \quad (5)$$

where $|u_j^{i,s}|$ and $\phi_j^{i,s}$ are controlled independently. Since in our experiment there is no spatial separation between idler and signal modes, we address each photon individually by assigning $M^i(\omega)$ to the lower-frequency part and $M^s(\omega)$ to the higher-frequency part of the spectrum. The measured signal after shaping and the up conversion stage then reads $S = |\int_{-\infty}^{\infty} d\omega\Gamma(\omega)M^i(\omega)M^s(-\omega)|^2$ for a continuous-wave pump and is equivalent to

$$S = |\langle\chi|\psi\rangle^{(d)}|^2 = \left|\sum_{l=0}^{d-1} u_l^i u_l^s c_l\right|^2 \quad (6)$$

for $|\chi\rangle = (\sum_{j=0}^{d-1} u_j^{i*}|j\rangle_i)(\sum_{j'=0}^{d-1} u_{j'}^{s*}|j'\rangle_s)$ with $|\psi\rangle^{(d)}$ of Eq. (4). The combination of the SLM together with an up

conversion coincidence detection therefore realizes a projective measurement. Different quantum information protocols can thus be implemented through a judicious choice of $|\chi\rangle$ together with Eq. (5).

IV. RESULTS

A. Quantum state tomography

At first, maximally entangled states are generated from Eq. (4) by Procrustean filtering [26]. Due to the characteristic shape of the SPDC spectrum (Fig. 1) a frequency-bin discretization entails unequal distributed probability amplitudes c_l. In order to equate the c_l and thus maximize the entanglement we discard photon combinations with high probabilities by adjusting the amplitudes $|u_j^{i,s}|$ in Eq. (5). Quantum-state tomography [28] then allows us to retrieve the density matrix $\hat{\rho}_d$ of these states by performing projective measurements [12] and using maximum likelihood estimation [29]. The reconstructed density matrices up to dimension $d = 4$ are shown in Fig. 2. The computed fidelities [30] F_d between the reconstructed state $\hat{\rho}_d$ and a maximally entangled state are $F_2 = 0.928 \pm 0.010$, $F_3 = 0.855 \pm 0.010$, and $F_4 = 0.781 \pm 0.018$. We estimated the statistical 2σ uncertainties with a Monte Carlo method by randomly adding normally distributed noise to each measurement outcome and recomputing the fidelity. With increasing dimension we have to implement more frequency bins within the same spectral range. Because of the finite spectral resolution of the setup, the increasing overlap between adjacent bins leads to a decrease of the fidelity.

B. Bell inequalities

More generally, we obtain nonmaximally entangled states by varying the amplitudes in $|\psi\rangle^{(d)}$. These states are then studied with regard to their nonlocal properties. Collins *et al.* (hereafter referred to as CGLMP) generalized Bell inequalities to arbitrary d-dimensional bipartite quantum systems by defining a dimensional-dependent Bell parameter I_d [3]. If correlations between two separated systems can be explained through local realism, then $I_d \leqslant 2$ holds for all $d \geqslant 2$. Despite a left-open locality loophole in our detection method, the violation of the precedent inequality indicates the existence of nonclassical correlations due to entanglement. A counterintuitive property of the CGLMP inequality is that for dimensions $d \geqslant 3$ the inequality is more strongly violated by certain nonmaximally entangled states than by maximally entangled states [4]. In order to compare the sensitivity of the Bell parameters $I_2(\gamma)$ and $I_3(\gamma)$ to an entanglement parameter $\gamma \in [0,1]$, we consider the following bipartite qubit and qutrit states:

$$|\psi(\gamma)\rangle^{(2)} = \frac{1}{\sqrt{1+\gamma^2}}(|0\rangle_i|0\rangle_s + \gamma|1\rangle_i|1\rangle_s), \tag{7}$$

$$|\psi(\gamma)\rangle^{(3)} = \frac{1}{\sqrt{2+\gamma^2}}(|0\rangle_i|0\rangle_s + \gamma|1\rangle_i|1\rangle_s + |2\rangle_i|2\rangle_s). \tag{8}$$

The Bell parameter itself is a combination of projection measurements and specific detection settings both explicitly given in Ref. [3]. It has been shown [4] for qutrits that the Bell inequality $I_3 \leqslant 2$ is maximally violated for $\gamma_{\max} = (\sqrt{11} - \sqrt{3})/2 \approx 0.792$. We measured the Bell parameters $I_2^{\text{expt.}}$ and $I_3^{\text{expt.}}$ for qubits and qutrits as a function of γ (Fig. 3). The reduced entanglement, i.e., $\gamma < 1$, is obtained by decreasing the transmission amplitudes of the bins associated with $|1\rangle_i|1\rangle_s$ using the SLM. The experiment reveals a higher sensitivity to γ of the Bell parameter for qubits compared to qutrits, which is in accordance with theoretical predictions. The theoretical curves are scaled to the experimental data using the symmetric noise model $\hat{\rho}_d^{\text{sn}}(\gamma) = \lambda_d|\psi(\gamma)\rangle^{(d)\,(d)}\langle\psi(\gamma)| + (1-\lambda_d)\mathbb{1}_{d^2}/d^2$ in which deviations from a pure state due to white noise are quantified by a mixing parameter λ_d and $\mathbb{1}_{d^2}$ denotes the d^2-dimensional identity operator. The value of the Bell parameter for $\hat{\rho}_d^{\text{sn}}(\gamma)$ then scales as $\lambda_d I_d(\gamma)$. Note that the specific detection settings are not optimal for $d = 2$. In Fig. 3, we therefore additionally depict values of the Bell parameter for optimal settings given by Horodecki's theorem [31]. Similar to the measured $I_2(\gamma)$ and in contrast to $I_3(\gamma)$, the Horodecki curve

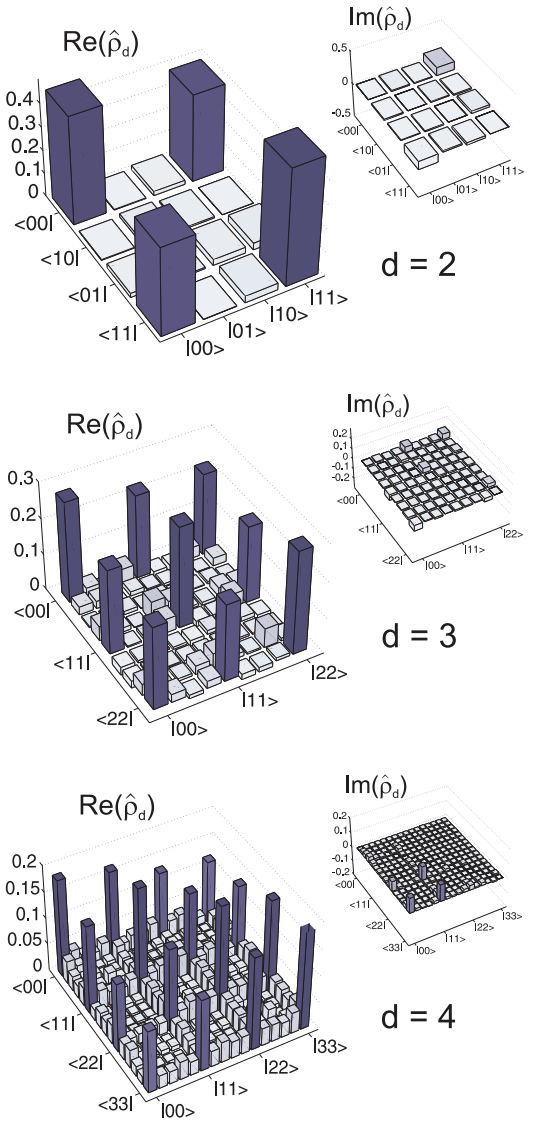

FIG. 2. (Color online) Reconstructed density matrices $\hat{\rho}_d$. From top to bottom: $\hat{\rho}_d$ of a qubit, qutrit, and a ququart, based on background-subtracted coincidence counts. Shown are the real and the imaginary parts. The small, residual imaginary values are due to remaining dispersion between the frequency bins.

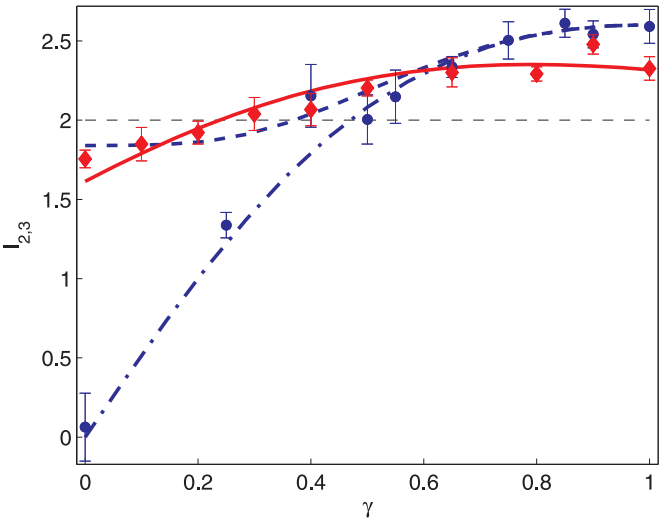

FIG. 3. (Color online) Bell parameter I_d in dependence of the entanglement parameter γ. The experimental Bell parameter $I_2^{\text{expt.}}$ is depicted with blue dots and $I_3^{\text{expt.}}$ with red diamonds. The 2σ uncertainties are calculated assuming Poisson statistics on background-subtracted coincidence counts. The theoretically predicted Bell parameters $I_2(\gamma)$ (dotted-dashed blue line), $I_2(\gamma)$ using the Horodecki theorem (dashed blue line), and $I_3(\gamma)$ (solid red line) are scaled with their corresponding mixing parameter. The (horizontal) dashed black line indicates the local variable limit. We experimentally determine the mixing parameters to be $\lambda_2^{\text{expt.}} = 0.920 \pm 0.013$ and $\lambda_3^{\text{expt.}} = 0.807 \pm 0.008$ with 2σ uncertainties.

is monotonically decreasing for $\gamma < 1$. In the $d = 3$ case the optimal settings were only determined for $\gamma = 1$ and $\gamma_{\max}$ [4].

V. CONCLUSION AND OUTLOOK

In conclusion, we have demonstrated coherent control of high-dimensional entanglement by performing quantum-state tomography for qudits up to $d = 4$ and Bell-test measurements for qubits and qutrits with a varying degree of entanglement. Since a broad class of transfer functions can be applied to the SLM, other qudit encoding schemes, such as time bins and realizations based on Schmidt modes, can be implemented. In our actual experiment, the available dimension to encode qudits in the frequency domain is limited by the setup's spectral resolution, the pixel size of the SLM, and the bandwidth of the pump laser in descending order. Improving the spectral resolution to match the pixel size of the SLM would allow for qudits with dimensions as high as a few hundred. Further, adapting the spectral resolution and the SLM pixel size to the bandwidth of the pump laser would allow for dimensions as high as a few million. Thus, this methodology provides a vast potential to test the fundamental aspects of quantum mechanics and is of great importance for many aspects of quantum information science.

ACKNOWLEDGMENTS

This research was supported by Grant No. PP00P2_133596 and by the NCCR MUST, both funded by the Swiss National Science Foundation.

[1] R. Horodecki, P. Horodecki, M. Horodecki, and K. Horodecki, Rev. Mod. Phys. **81**, 865 (2009).
[2] A. Zeilinger, Rev. Mod. Phys. **71**, 288 (1999), and references therein.
[3] D. Collins, N. Gisin, N. Linden, S. Massar, and S. Popescu, Phys. Rev. Lett. **88**, 040404 (2002).
[4] A. Acín, T. Durt, N. Gisin, and J. I. Latorre, Phys. Rev. A **65**, 052325 (2002).
[5] T. Vértesi, S. Pironio, and N. Brunner, Phys. Rev. Lett. **104**, 060401 (2010).
[6] L. Sheridan and V. Scarani, Phys. Rev. A **82**, 030301 (2010).
[7] P. G. Kwiat, E. Waks, A. G. White, I. Appelbaum, and P. H. Eberhard, Phys. Rev. A **60**, R773 (1999).
[8] A. C. Dada, J. Leach, G. S. Buller, M. J. Padgett, and E. Andersson, Nat. Phys. **7**, 677 (2011).
[9] H. Di Lorenzo Pires, C. H. Monken, and M. P. van Exter, Phys. Rev. A **80**, 022307 (2009).
[10] A. Mair, A. Vaziri, G. Weihs, and A. Zeilinger, Nature (London) **412**, 313 (2001).
[11] N. K. Langford, R. B. Dalton, M. D. Harvey, J. L. O'Brien, G. J. Pryde, A. Gilchrist, S. D. Bartlett, and A. G. White, Phys. Rev. Lett. **93**, 053601 (2004).
[12] M. Agnew, J. Leach, M. McLaren, F. S. Roux, and R. W. Boyd, Phys. Rev. A **84**, 062101 (2011).
[13] R. Fickler, R. Lapkiewicz, W. N. Plick, M. Krenn, C. Schaeff, S. Ramelow, and A. Zeilinger, Science **338**, 6107 (2012).
[14] D. Giovannini, F. M. Miatto, J. Romero, S. M. Barnett, J. P. Woerdman, and M. J. Padgett, New J. Phys. **14**, 073046 (2012).
[15] C. K. Law, I. A. Walmsley, and J. H. Eberly, Phys. Rev. Lett. **84**, 5304 (2000).
[16] C. K. Law and J. H. Eberly, Phys. Rev. Lett. **92**, 127903 (2004).
[17] Yu. M. Mikhailova, P. A. Volkov, and M. V. Fedorov, Phys. Rev. A **78**, 062327 (2008).
[18] R. T. Thew, A. Acín, H. Zbinden, and N. Gisin, Phys. Rev. Lett. **93**, 010503 (2004).
[19] D. Richart, Y. Fischer, and H. Weinfurter, Appl. Phys. B **106**, 543 (2012).
[20] L. Olislager, J. Cussey, A. T. Nguyen, P. Emplit, S. Massar, J.-M. Merolla, and K. P. Huy, Phys. Rev. A **82**, 013804 (2010).
[21] A. Hayat, X. Xing, A. Feizpour, and A. M. Steinberg, Opt. Express **20**, 29174 (2012).
[22] A. M. Weiner, Rev. Sci. Instrum. **71**, 1929 (2000).
[23] A. Pe'er, B. Dayan, A. A. Friesem, and Y. Silberberg, Phys. Rev. Lett. **94**, 073601 (2005).
[24] F. Zäh, M. Halder, and T. Feurer, Opt. Exp. **16**, 16452 (2008).
[25] S. Lerch, B. Bessire, C. Bernhard, T. Feurer, and A. Stefanov, J. Opt. Soc. Am. B **16**, 953 (2013).
[26] C. H. Bennett, H. J. Bernstein, S. Popescu, and B. Schumacher, Phys. Rev. A **53**, 2046 (1996).
[27] T. P. Wihler, B. Bessire, and A. Stefanov, arXiv:1209.2575.
[28] R. T. Thew, K. Nemoto, A. G. White, and W. J. Munro, Phys. Rev. A **66**, 012303 (2002).
[29] Z. Hradil, Phys. Rev. A **55**, R1561 (1997).
[30] R. Jozsa, J. Mod. Opt. **41**, 2315 (1994).
[31] R. Horodecki, P. Horodecki, and M. Horodecki, Phys. Lett. A **200**, 340 (1995).